# NATIONAL ADVISORY COMMITTEE FOR AERONAUTICS

**TECHNICAL NOTE 3518** 

ROTATING -STALL CHARACTERISTICS OF A ROTOR

WITH HIGH HUB-TIP RADIUS RATIO

By Eleanor L. Costilow and Merle C. Huppert

Lewis Flight Propulsion Laboratory Cleveland, Ohio



Washington August 1955

#### TECHNICAL NOTE 3518

## ROTATING-STALL CHARACTERISTICS OF A ROTOR

#### WITH HIGH HUB-TIP RADIUS RATIO

By Eleanor L. Costilow and Merle C. Huppert

#### SUMMARY

The rotating-stall characteristics of a 0.9 hub-tip ratio rotor were investigated. Stall patterns consisting of two, three, and one total-span stall zones developed in that order upon reduction of flow coefficient. The one-stall-zone pattern caused the most severe pressure, temperature, and flow fluctuations.

As the flow decreased within the stall zone, detailed measurements showed an increase in static pressure within the stall zone upstream of the rotor and a static-pressure decrease downstream of the rotor. These pressure fluctuations were of sufficient amplitude in the case of the one-stall-zone pattern to result in a pressure drop across the rotor within the stall zone.

All stall zones rotated in the direction of rotor rotation relative to the compressor casing and at a speed proportional to but less than rotor speed. The measured stall-propagation rates were compared with those predicted by theory. The relative stall-propagation rate increased with increasing stall-zone size.

#### INTRODUCTION

Four extensive experimental investigations reported in references 1 to 4 show that stall in axial-flow and centrifugal compressors may manifest itself in asymmetric flows. This type of stalled condition has come to be known as propagating or rotating stall (ref. 4 refers to the phenomenon as "type 1 surge"). The asymmetric flows consist of one or more low-flow regions encompassing several blade passages. These low-flow regions rotate about the compressor at a speed proportional to but less than rotor speed and in the direction of rotor rotation relative to an absolute frame of reference.

NACA TN 3518

When rotating stall is encountered, an abrupt decrease in compressor pressure rise may occur when a single total-span stall zone develops. This type of stall is often called abrupt stall. The compressor then operates on a stalled branch of the compressor performance characteristic as shown in figure 1(a). Upon increasing the weight flow, the compressor recovers from the severe stalled condition at a higher weight flow than that where the drop in pressure originally occurred, thus forming the hysteresis loop indicated in figure 1(a). Reference 4 reports two stalled branches for one compressor; however, the data indicate that a compressor usually has one preferred stalled operating characteristic at any given speed. References 1 to 4 report some compressor configurations where a continuous performance characteristic similar to that shown in figure 1(b) is obtained when rotating stall is present. Generally, in these cases only a portion of the blade span is stalled. This type of stall is often called partial-span or progressive stall.

3683

In addition to the effect of rotating stall upon performance, reference 5 suggests that rotating stall is a source of resonant excitation that may result in blade failure. Compressor blade failures directly attributable to rotating stall are reported in reference 6.

The flow fluctuations associated with rotating stall are distinctly different from the phenomenon generally called "surge." During operation with rotating stall, the net flow rate through the compressor and the torque necessary to drive the compressor remain essentially constant, whereas these quantities fluctuate during surge.

The problem of rotating stall in a single blade row is analyzed in references 7 to 10. In references 7 to 9 the blade row is considered to have an infinitesimal chord length (actuator sheet), whereas the effect of blade chord is included in reference 10. The analyses show qualitatively that flow patterns of the rotating-stall type may occur in axisymmetric rigid blade rows with steady uniform inflow to the blade row.

To obtain a better understanding of the stall phenomenon, an investigation of the rotating-stall characteristics of a 0.9 hub-tip ratio rotor has been carried out at the NACA Lewis laboratory. The high hub-tip ratio rotor is typical of an exit stage of a multistage compressor and corresponds approximately with the two-dimensional single-blade-row models considered in the theoretical treatments. The investigation was made in order to provide more detailed information regarding the stall mechanism, pressure, temperature, and flow fluctuations and their axial extent, and the phasing relation of the fluctuations. Results are compared with theoretical analyses where applicable.

## I-1 back

#### APPARATUS AND INSTRUMENTATION

#### Rotor Design and Installation

The 14-inch-diameter rotor used in this investigation has 31 aluminum blades of 0.9 hub-tip ratio. The blades are untwisted and untapered. NACA 65(12)-10 blower blade profiles were used. The rotor blade setting angle was 28.5°, and the inlet-air angle for minimum losses as determined from cascade tests was 45°. Figure 2 shows the design vector diagram.

The rotor test setup is shown schematically in figure 3. Air entered through the orifice tank and a motor-driven inlet throttle into an inlet tank where screens were used to straighten the air at the compressor inlet. The compressor air discharged into a receiver and then through an outlet throttle to the laboratory altitude exhaust system.

#### Flow-Fluctuation Instrumentation

A constant-temperature hot-wire-anemometer system such as reported in references 11 and 12 was used to measure flow fluctuations. The wire element of the anemometer probe was made of 0.0002-inch-diameter tungsten wire mounted parallel to the probe axis and oriented in the stream so that the wire element was not in the wake of its supports. The anemometer output signal was filtered electronically to pass up to 2000 cps and recorded photographically from a dual-beam direct-coupled cathode-ray oscilloscope.

Hot-wire-anemometer probes were installed at axial stations 2, 4, 5, 6, 7, and 8 (fig. 4). Probes were installed at several angular spacings at station 4.

#### Pressure-Fluctuation Instrumentation

Pressure fluctuations during stall were measured with a calibrated inductance-type pressure pickup of the kind reported in reference 13. For the purpose of the investigation, the pressure pickup was installed in the compressor casing as shown in figure 5. The pressure pickups were inserted into the compressor casing with the static tap flush with the inner surface of the compressor casing at axial stations 3 and 7 (fig. 4). Radial measurements were obtained from "extension disks" from the static tap. The amplitude response of the pickup was "flat" to a frequency of 1000 cps (ref. 13), which was well above the stall frequencies encountered. The output of the pickup was photographically recorded from a dual-beam direct-coupled cathode-ray oscilloscope.

## Temperature-Measurement Instrumentation

The average temperature rise across the rotor row was measured by iron-constantan thermocouples mounted in stagnation shields at axial stations 4 and 7. The temperature fluctuations during rotating stall were measured at axial stations 4 and 7 by a compensated thermocouple made of chromel-constantan 0.003 inch in diameter and also with a 0.0002-inch-diameter tungsten-wire resistance thermometer. Both of these devices are discussed in reference 14. The resistance-thermometer and compensated-thermocouple outputs were viewed on a dual-beam oscilloscope.

#### PROCEDURE

#### Rotor Performance Characteristic

The steady-state performance of the rotor is expressed in terms of pressure and flow coefficients. The curve showing the relation between these two parameters is referred to as the static performance characteristic. The pressure and flow coefficients, as defined in the symbol list of appendix A, were determined from data from 35 static-pressure taps along the inner and outer casings and from the weight flow and temperature. The flow coefficient was varied from choked flow to a low-flow condition by means of the outlet throttle.

Investigation over several speeds showed that the stall zones rotated at a speed proportional to the rotor speed. The data reported herein were taken at  $N/\sqrt{\theta} = 8000$  rpm (rotor tip speed of 500 ft/sec). An absolute inlet tank pressure of 25 inches of mercury was maintained at all weight flows.

Measurement of Flow, Pressure, and Temperature Fluctuations

The voltage output of the hot-wire anemometer was converted into mass-flow fluctuations by the method of appendix B. The number of stall zones was found by displacing hot-wire probes around the circumference at several different angular spacings at axial station 4 and applying the analysis of appendix B. The stall frequency was determined by forming Lissajous figures on the oscilloscope with an audio-frequency oscillator.

The amplitudes of the static-pressure and total-temperature fluctuations were measured at axial stations 4 and 7 (fig. 4) for each stall pattern obtained, along with the flow fluctuations at axial stations 2, 4, 5, 6, 7, and 8.

#### Performance and Stall Characteristics

The static performance characteristics for the annulus between stations 1 and 5, for the rotor between stations 5 and 6, and for the complete unit between stations 1 and 6 are given in terms of pressure and flow coefficient in figure 6. While the pressure coefficients for the inlet annulus and for the complete unit continue to rise upon reduction of flow coefficient, the pressure coefficient for the rotor begins to fall off at approximately  $\varphi = 0.9$ , until at  $\varphi = 0.75$  a rotating-stall pattern of two zones develops. At this point the over-all performance as well as the rotor performance is affected by the rotating-stall condition. However, the amplitude of the flow fluctuation is not of sufficient magnitude to affect the pressure coefficient of the inlet annulus. Upon further reduction in flow coefficient, a three-stall-zone pattern develops at  $\varphi = 0.69$  and persists to a flow coefficient of 0.64, where a single stall zone covering about one-third of the annulus and producing large flow fluctuations develops. The single-zone stall pattern has a considerable effect on the inlet-annulus and over-all pressure coefficients. The single rotating-stall zone remained through a flow coefficient of 0.52. The valve arrangement of the system did not permit flow coefficients between zero and 0.52 to be obtained conveniently, so no data were taken in this flow-coefficient range.

The rotor was run for a short time with the valve completely closed to determine the rotating-stall characteristics at zero weight flow. One stall zone was found rotating at half rotor speed.

The rotating-stall patterns are summarized as follows for a rotational speed N of 136 rps:

Range of flow coefficient,	Number of stall zones,	Frequency of stall zone passing hotwire probe, $f_{\rm s}$ , cps	Rotational speed of stall zones, h, rps	Ratio of stall-zone speed to rotor speed, h/N	
0.75 - 0.69 .6964 .6452	2 3 1 1	175 276 60 68	87.5 92.0 60.0 68.0	0.64 .68 .44 .50	

If the rotor were operated at the flow coefficient of 0.52 for several minutes, the stall pattern would change from  $\lambda=1$  to  $\lambda=4$ . The four stall zones might then later regroup into the original one zone.

This breaking down into four zones would recur on subsequent operation at this point, indicating that the one stall zone was not unique at this point even though it was the first to appear.

#### Rotor Pressure-Rise Coefficient

The two-dimensional pressure characteristic of the rotor at midspan (r=0.95) in terms of cascade parameters is given in figure 7. The pressure-rise coefficient  $\Delta p/q_m$  increases until an inlet angle of  $50^\circ$  is reached and then remains constant until approximately  $52^\circ$ , where rotating stall is encountered and the pressure-rise coefficient decreases. Because the flow is fluctuating with time, the pressure rise measured during operation with rotating stall is a time-averaged value and not necessarily the true static characteristic. Since rotating stall produces alternating high- and low-flow areas, the inlet angle also oscillates over a wide range.

The rotor pressure rise obtainable assuming two-dimensional, isentropic, compressible flow and a constant exit angle of  $22\frac{1}{2}^{0}$  is also given in figure 7. The slope of the curves is the same except where the inlet angle deviates more than  $5^{0}$  from the design angle. The rotor pressurerise coefficient is approximately 75 percent of the isentropic value at the design inlet angle. The rotor blade choked at an inlet angle of approximately  $36^{0}$  and a relative inlet Mach number of about 0.73, as is indicated by the sharp reduction in pressure-rise coefficient.

#### Flow Fluctuations due to Rotating Stall

Variation in amplitude of flow fluctuations with axial position. Flow fluctuations caused by rotating stall are shown in figure 8. The average flow fluctuations are reported at the mean radius (r = 0.95). In general, the anemometer signal obtained at station 6 was too "hashy" to analyze quantitatively for flow-fluctuation amplitudes, and no data are reported for this station. As may be seen from figure 8, the flow fluctuations for  $\lambda = 1$  were the most severe and of nearly the same amplitude at all axial measuring stations. The fluctuations for two-and three-zone stall patterns were largest near the rotor and diminished in amplitude both upstream and downstream of the rotor.

Representative oscillograms from axial surveys are reproduced in figure 9. Multiple traces appear on some of the oscillograms, because the oscilloscope beam swept more than once during the film exposure time. All the traces appear in pairs with one anemometer trace from station 4, selected for comparison. The oscillograms in figures 9(a) and (b) for

NACA TN 3518

the two- and three-stall patterns, respectively, show clearly the small-amplitude flow fluctuations upstream and the relatively larger fluctuations in the downstream annulus. Where one stall existed (fig. 9(c)), the flow fluctuations were of nearly the same amplitude at all stations, with little change in wave shape downstream of station 2.

Variation in amplitude of flow fluctuation along blade span. - As might be expected for a short blade height, flow fluctuations caused by rotating stall existed over the entire blade span for all rotating-stall patterns. The results of a radial survey at station 5 immediately preceding the rotor are given in figure 10. The three-stall-zone pattern exhibited the greatest radial variation in fluctuation amplitude. The fluctuations become more equally distributed spanwise as the number of stall zones is reduced. The flow fluctuations with one stall zone are uniformly distributed over the entire span and as pointed out earlier are of much greater amplitude than either the two- or three-stall-zone flow fluctuations.

Typical oscillograms from the radial surveys at station 5 are given in figure 11 for the two-, three-, and one-stall patterns. There is a pronounced change in wave shape between the two- and three-stall-zone patterns of figures 11(a) and (b) and that for the one-stall pattern in figure 11(c).

It seems altogether likely that some reversed flow took place near the rotor with the single-zone stall pattern. The upswing within the stall-zone "blip" on figure ll(c) may be an indication of reversed flow. Reversed flow or back flow within the stall zone is sometimes observed (e.g., ref. 4). Such observations are usually made by detecting the motion of tufts mounted upstream or downstream of the compressor with stroboscopic light. Since the anemometer probes used in this investigation are insensitive to flow direction, reversed flow could not be positively identified.

## Pressure Fluctuations due to Rotating Stall

Radial surveys with the pressure pickup at stations 3 and 7 indicated that the pressure variations during stall were essentially constant over the radius for all stall patterns. Typical oscillograms of the pressure fluctuations are shown in figure 12. For all stall patterns, the amplitude of the pressure fluctuations downstream of the rotor was approximately 60 percent of the upstream fluctuations. The highest-amplitude fluctuations occurred for the single-zone stall pattern (fig. 12(c)). The pressure fluctuations at stations 3 and 7 were nearly 180° out of phase, as shown by the oscillogram in figure 13, which was obtained during operation with the single-zone stall pattern.

The pressure fluctuations at stations 3 and 7 are shown schematically in figure 14. The two- and three-zone stall patterns produced approximately a ±10-percent variation in pressure rise between stations 3 and 7. The single-zone stall pattern, however, resulted in a much greater variation, as shown in figure 14(c). The maximum static pressure at station 3 during operation with the single-zone stall pattern was slightly greater than the inlet total pressure (station 1); the minimum pressure at station 7 was only slightly greater than the average pressure at station 3. That is, within the stall zone the static pressure at station 3 was increased to approximately the inlet stagnation pressure, while the static pressure at station 7 decreased to a value slightly greater than the average static pressure at station 3. Within the stall zone there was a pressure drop across the rotor. This drop is shown in terms of pressure coefficient in figure 15, where the instantaneous pressure coefficient between stations 3 and 7 is plotted against time.

The hot-wire-anemometer data obtained during operation with the single-zone rotating-stall pattern indicated that the flow coefficient at station 4 varied from nearly zero in the stall zone to a value between 0.85 and 0.92 between stall zones. The uncertainties involved in interpreting the anemometer data prevent a more accurate determination of the flow coefficient between stall zones. The steady-state or static performance of the rotor and inlet annulus is shown in figure 16 in terms of pressure coefficient for comparison with the instantaneous pressure coefficients obtained with the single-zone stall pattern. According to figure 14(c), the maximum pressure coefficient across the rotor  $\psi_{z_{-7}}$ was 0.805 and the minimum pressure coefficient in the inlet annulus  $\psi_{1-3}$ was -0.784. These values correspond to a flow coefficient  $\varphi$  of 0.87 on the static performance curves in figure 16, compared with a flow coefficient between 0.85 and 0.92 estimated from the anemometer data. The maximum pressure coefficient  $\psi_{3-7}$  outside the stall zone for the single-zone stall pattern is therefore approximately the same as the maximum steadystate (unstalled) pressure coefficient.

Inasmuch as the flow fluctuations obtained with the two- and three-zone stall patterns were somewhat smaller than those with the single-zone stall pattern, the fluctuations in pressure coefficient were correspondingly less, as indicated in figures 14(a) and (b).

The data indicate that the pressure coefficients between stall zones correspond approximately to the steady-state values at the steady-state flow rate. A similar comparison for conditions within the stall zone cannot be made, because steady-state data at low (stalled) flows were not obtainable.

## Temperature Fluctuations due to Rotating Stall

The measured average temperature rise across the rotor is plotted against flow coefficient in figure 17. The temperature rise increases rapidly at low flow coefficients where rotating stall is encountered. The amplitude of the temperature fluctuations at station 7 during rotating stall was 4° F for the two- and three-stall patterns and 25° F for the single-zone stall pattern.

Figure 18 represents the approximate fluctuation in total temperature at station 7 during operation at a flow coefficient of 0.63 with the single-zone stall pattern. The average temperature rise under these conditions is 23° F (fig. 17). The minimum temperature rise occurring in the flow area outside the stall zone is 16° F, and the maximum rise in the stall zone is 41° F.

The analysis of the pressure oscillograms and anemometer signals indicated the through-flow velocity in the stall zone to be essentially zero. Assuming, then, that the air in the blade passages lying within the stall zone rotates at blade speed, the temperature rise across the rotor in the stall zone would be

$$\Delta T_{5-7} = \frac{U_{\rm m}^2}{\rm gJc_p} = \frac{(475)^2}{6000} = 38^{\circ} \text{ F}$$

which is in good agreement with the measured value of 41°F. The quasisteady-state analysis indicated a flow coefficient of 0.87 outside the stall zone. Under steady flow conditions at this flow coefficient, a temperature rise of 18°F was measured (fig. 17), which is close to the 16°F temperature rise measured at the same flow coefficient under unsteady flow conditions.

## Discussion of Rotating Stall and Comparison with Theory

The mechanism by which the stall zones propagate from blade to blade is usually explained in a qualitative manner as follows. Consider an infinite row of blades operating at the stall point in two-dimensional flow (see fig. 19). Now suppose that a small perturbation in the incoming flow causes blade 2 to stall and consequently become incapable of supporting the existing pressure rise across the blade row. As a consequence of stall, the flow will be reduced through the separated blade passage. The incoming flow will be diverted around the local low-flow area, and hence the angle of attack on blade 3 will increase while the angle of attack on blade 1 will decrease. Blade 3 will stall, and the low-flow or stall zone will propagate in the direction of the component of velocity parallel to the cascade. After a fraction of a second, the

3683

CI-2

stall-zone propagation rate and size would presumably reach some equilibrium value covering several blade passages. For an annular cascade, the stall zone would propagate around the axis of the cascade and is thus called rotating stall.

The rotor used in this investigation corresponds approximately to this model. The hub-tip ratio is 0.9, so that the flow is nearly two-dimensional. Relative to the rotor, the stall zones propagate in the direction of the tangential velocity but at a velocity less than the rotor speed, so that in an absolute sense the stall zones rotate in the direction of the rotor rotation.

The qualitative explanation of stall propagation gives the correct direction of rotation of the stall zones and also implies the increase in static pressure within the stall zone ahead of the blade row. This explanation also implies that operation at the stall point is unstable. If the flow were stable, the perturbation would be damped and steady rotating stall would not be obtained.

A prediction or estimation of the rotative speed of the stall pattern and the number of zones formed requires additional considerations. References 7 to 10 present linearized analyses that result in expressions for the stall-propagation rate. There are no methods available for estimating the number of stall zones that will form. The theories consider two different forms of a single blade row. Marble (ref. 9) and Sears (refs. 7 and 8) represent the blade row by an infinite number of small-chord blades, so that the configuration they use is in effect an actuator sheet. Stenning (ref. 10) considers a cascade of blades of finite chord length.

Sears considers a flow represented by an irrotational flow field entering the rotor, an actuator sheet acting as the rotor, and a rotational field leaving the rotor. The vorticity following the actuator sheet is determined either from consideration of the shedding of vortices by the blades as they pass through the stall zones ("airfoil theory") or from the variation in downstream total pressure ("channel theory").

In the airfoil theory, expressions are derived for the blade circulation in terms of the velocity distribution. The induced inflow velocities at the actuator sheet are calculated from the shed vorticity. After introducing a phase angle  $\Delta$  between lift and angle of attack, the conditions required for the blade-loading variations to be just supported by the induced velocities are determined. The conditions required are as follows:

$$\frac{-m\sigma}{4} = \frac{\left[\cot^{2}\beta + \left(\frac{h}{N}\right)^{2}\right]\cos\Delta}{\left(1 - \frac{h}{N}\right)^{2}\cos\beta} \tag{1}$$

$$\frac{h}{N} = \left(1 + \frac{\tan^2 \beta - 1}{2 \tan \beta \tan \Delta}\right) \pm \sqrt{1 + \frac{\tan^2 \beta - 1}{2 \tan \beta \tan \Delta}^2 + \frac{2}{\tan \beta \tan \Delta} - 1}$$
 (2)

In order for stall propagation to occur with the slope of the lift curve m just slightly negative, the phase shift  $\Delta$  must approach  $90^{\circ}$ . The experimental stall-propagation rates are compared with those obtained considering the negative root of equation (2) in figure 20. The phase-shift values  $\Delta$  required for close agreement with the data are  $80^{\circ}$  and  $85^{\circ}$ , as seen from figure 20. At zero weight flow ( $\beta = 90^{\circ}$ ), the theory would predict either no stall or a stall propagating at rotor speed, since h/N is zero. Experimentally, a value of h/N = 0.50 was obtained.

The channel theory (ref. 8) utilizes relations derived from cascade tests - namely, that the relative outlet-air angle and the pressure rise across the blade row are functions of the inlet-air angle. The induced velocities are calculated from the variation in total pressure downstream of the rotor. A phase angle  $\delta$ , similar to that used in the airfoil theory, is introduced; and the procedure used in the analysis is much the same as for the airfoil theory. The conditions required for the downstream total-pressure variation to be just supported by the induced velocities are as follows:

$$M = \sqrt{1 + \left(\frac{h}{N}\right)^2 \tan^2\beta} \, (\sec^2\beta) \tag{3}$$

$$\frac{h}{N} = -\cot \beta \cot (\delta + 2\beta) \tag{4}$$

A plot of equation (4) for  $\delta$  of  $0^{\circ}$ ,  $10^{\circ}$ , and  $20^{\circ}$  is shown in figure 21. (The  $\delta = 0^{\circ}$  curve will be discussed further in connection with Marble's theory.) Values of  $\delta$  of  $10^{\circ}$  and  $20^{\circ}$  bring the channel theory in reasonable agreement with all the data except at a flow coefficient of zero, in which case a phase shift of zero is required for agreement between theory and experiment.

Marble in reference 9 like Sears in reference 8 represents the blade row as an actuator sheet. The pressure-rise curve across the disk is assumed to be a linear function of the inlet-air angle for unstalled flow and to drop discontinuously to zero for stalled flow. Pressure is used as the dependent variable in the analysis instead of the velocity components used by Sears. The asymmetric flow is introduced by considering a stall zone of variable circumferential extent to exist in the actuator disk. Two cases are considered: a "simple cascade" solution, where the deviation angle remains constant for all values of incidence angle, and a "general cascade characteristics" solution, where the cascade pressure rise and the deviation angle are considered functions of the incidence angle. A phase angle between angle of attack and pressure rise is not considered. If the phase angle  $\delta$  is assumed zero in Sears' channel

3683

theory, the expressions for stall-propagation rate obtained by Marble for the simple cascade and by Sears are identical. This relation is shown in figure 21. In addition to propagation rate, Marble finds an expression for stall-zone width.

The stall analysis by Stenning (ref. 10) considers a cascade of finite chord length. It is assumed that the effective outlet area of the blade passage is reduced (flow coefficient reduced) as a result of stall and that the flow coefficient of the blade passages is determined by the inlet angle. The static pressure is assumed constant downstream of the cascade in spite of the asymmetric flow pattern. The data obtained in the present investigation indicate that the downstream static pressure is not a constant. The effect of the variation in downstream static pressure on propagation rate has, however, not been ascertained. Stenning obtains a solution for the stall-propagation rate from momentum considerations within the cascade. The result obtained where the blade row is assumed to consist of a large number of short-chord blades is

$$1 - \frac{h}{N} = \frac{\cot^2 \beta}{\kappa^2 \cos^2 \gamma} \tag{5}$$

One of the results of Stenning's work considering the finite-chordlength blade row is that the relative stall-propagation rate increases with the size of the stall zone. The experimental results of the present investigation agree with this conclusion, as shown in figure 22. In this figure the relative propagation rate is plotted as a function of the ratio of blade chord to stall-zone width. As the stall-zone width increases (i.e., smaller values of c/z), the propagation rate increases, as Stenning predicted. Extrapolating the experimental curve to c/z = 0corresponds to the actuator disk Marble and Sears studied (one of infinitely small chord). The values of stall-propagation rate obtained from the Sears theories are shown at c/z = 0 for comparison. The stallpropagation rates obtained from the Sears channel theory (eq. (4)) with a phase shift  $\delta$  of  $5^{\circ}$  and  $\beta$  of  $60^{\circ}$  and from the airfoil theory (eq. (2)) with a phase shift  $\Delta$  of 80° and  $\beta$  of 60° are in good agreement with the extrapolated data. A x value of 0.824 is required to make Stenning's predicted propagation rate (eq. (5)) agree at c/z = 0 for  $\beta = 60^{\circ}$  and  $\gamma = 22\frac{1}{2}^{\circ}.$ 

#### SUMMARY OF RESULTS

The rotating-stall characteristics of a 0.9 hub-tip ratio rotor were investigated, with the following results and observations:

1. As the flow coefficient was reduced, total-span stall zones developed in the following order: two zones, three zones, and one zone.

NACA TN 3518

The one-stall-zone pattern, which produced the most severe pressure, temperature, and flow fluctuations, spread over approximately one-third of the annulus.

- 2. The rotor performance in the flow area between the stall zones was in good agreement with that obtained under steady-state conditions at the same flow.
- 3. Static-pressure fluctuations downstream of the rotor were about 60 percent as large as and approximately 180° out of phase with the pressure fluctuations upstream of the rotor.
- 4. The relative stall-propagation rates increased with increasing stall-zone size.
- 5. The measured stall-propagation rates can be made to agree with theoretical predictions by adjusting certain theoretically undetermined factors appearing in the theories.

Lewis Flight Propulsion Laboratory
National Advisory Committee for Aeronautics
Cleveland, Ohio, June 13, 1955

## APPENDIX A

## SYMBOLS

The following symbols are used in this report:

	and a special series of the se						
$c_1, c_2$	constants in equation for heat-transfer characteristics of hot- wire anemometer (eq. (B12))						
С	blade chord						
cp	specific heat at constant pressure						
е	voltage drop across hot-wire anemometer, v						
e <sub>0</sub>	voltage drop across hot-wire anemometer with zero flow, v						
f()	indicates functional relation with quantity in parentheses						
f	frequency with which disturbance passes hot-wire anemometer or pressure transducer, cps						
g	acceleration due to gravity, ft/sec2						
h	absolute rotative speed of a propagating-stall zone, rps						
i	current through hot-wire anemometer, amp						
J	mechanical equivalent of heat, ft-lb/Btu						
k,n	integers (appendix B)						
M	slope of curve of rotor total-pressure-rise coefficient against inlet angle						
m	slope of curve of blade lift coefficient against inlet angle						
N	compressor rotative speed, rps or rpm as indicated						
p	static pressure, lb/sq ft						
q.	$\frac{1}{2}$ o $W^2$ , lb/sq ft						
r	ratio of local radius to rotor tip radius						
T	total temperature, <sup>O</sup> F						

```
U
         rotor blade speed, ft/sec
V
         absolute velocity, ft/sec
W
         relative velocity, ft/sec
X
         time between appearance of a flow fluctuation on oscillogram
           from one of two anemometers and appearance of a flow fluctu-
           ation on other anemometer (see fig. 23), sec
         xf
y
         width of stall zone
Z
         angular displacement between two hot-wire anemometers, deg
         relative inlet air angle measured from axial direction, deg
         relative outlet air angle measured from axial direction, deg
r
         denotes finite difference of quantity following
Δ
         phase-shift angle (refs. 7 and 8), deg
Δ
8
         phase-shift angle (ref. 8), deg
         ratio of compressor-inlet temperature to NACA standard sea-
           level temperature of 518.70 R
         effective blade passage area reduction (ref. 10)
×
λ
         number of stall zones in annulus
         angular displacement between two propagating-stall regions, deg
         density, slugs/cu ft
ρ
         mass-flow rate indicated by average current through hot wire,
Va
           lb/(sec)(sq ft), (eq. (B17))
DQ/VQL
         amplitude of flow fluctuation divided by PV
         cascade solidity
O
         flow coefficient, Vz/Um
```

```
3683
```

```
pressure coefficient, \Delta p/(\rho U_m^2/2)
         resistance of hot-wire anemometer, ohms
Subscripts:
         effective gas
         used to associate value of \alpha and possible corresponding
           values of \lambda
         mean radius (r = 0.95)
         stall
         hot-wire anemometer
         axial
Z
1,2,
. . .8 axial stations (fig. 4)
Presubscripts:
0,1,
         indicates value of n used in determining \lambda (see appendix B)
Superscripts:
         indicates clockwise rotation of propagating stall
         indicates counterclockwise rotation of propagating stall
         indicates differentiation
```

(bar) time-averaged value

#### APPENDIX B

## METHOD OF DETERMINING NUMBER OF STALL ZONES AND AMPLITUDE

## OF FLOW FLUCTUATIONS DUE TO ROTATING STALL

### Number of Stall Zones

In order to derive the expression necessary to determine the number of stalled regions by use of two anemometers displaced angularly in the plane of instrumentation (fig. 23(a)), it will be convenient to assume that the number of stalls and their direction of rotation are known.

A stalled region passes each anemometer station f times per second, and

$$f = h\lambda$$
 (B1)

The output signals of the two anemometers displaced angularly  $\alpha$  degrees appear on the oscilloscope as shown in figure 23(b). If the stalled regions are rotating clockwise as indicated in figure 23(a), a stall zone will pass each anemometer every 1/f second, and a given stall zone will first pass anemometer 1 and then pass anemometer 2 at  $\alpha/360h$  seconds later. Inasmuch as the stalls are quite similar, one stall zone cannot be distinguished from another, so  $\alpha/360h$  cannot, in general, be determined from a single oscillogram. The phase shift (i.e., the time x) can be read directly from the oscillogram. For the example shown,

$$x = \frac{\alpha}{360h} - \frac{1}{f}$$
 (B2)

Then the ratio  $\frac{x}{1/f} = \frac{\alpha f}{360h} - 1 = y$ .

Since

$$v = \frac{360}{\lambda} = \frac{360h}{f}$$

then

$$y = \frac{\alpha}{\nu} - 1 \tag{B3}$$

If there are twice as many stalled regions,

$$x = \frac{\alpha}{360h} - \frac{2}{f}$$

$$y = \frac{\alpha}{\nu} - 2$$

Then, in general, with the stalls rotating in the direction shown in figure 23(a),

$$x = \frac{\alpha}{360h} - \frac{n}{f}$$

and

$$y = \frac{\alpha}{y} - n \tag{B4}$$

where n is the number of stalls enclosed in angle  $\alpha$  and consequently an integer. The value of y then varies with  $\alpha/\nu$  as shown in figure 23(c). When equation (B4) is differentiated with respect to  $\alpha$ ,

$$\frac{\mathrm{dy}}{\mathrm{d\alpha}} = \frac{1}{\nu} = \frac{\lambda^+}{360} \tag{B5}$$

is obtained, provided  $\alpha/\nu$  is not an integer, in which case the derivative does not exist in the usual sense because y is discontinuous at these points.

If the stalls are rotating in the direction opposite (counter-clockwise) to that indicated in figure 23(a), a stall will pass anemometer 2 before passing anemometer 1. For counterclockwise rotation, the oscillograms would appear as shown in figure 23(d). In this case,

$$x = \frac{2}{f} - \frac{\alpha}{360h}$$

and

$$y = 2 - \frac{\alpha}{\nu} \tag{B6}$$

If there are twice as many stalls,

$$y = 3 - \frac{\alpha}{\nu}$$

and, in general,

$$y = n + 1 - \frac{\alpha}{y} \tag{B7}$$

A plot of y against  $\alpha/\nu$  is shown in figure 23(e), where n is, as before (eq. (B4)), the number of stalls enclosed in angle  $\alpha$  and consequently an integer. Differentiation of (B7) with respect to  $\alpha$  gives

$$\frac{\mathrm{dy}}{\mathrm{d\alpha}} = -\frac{1}{\mathbf{v}} = -\frac{\lambda^{-}}{360} \tag{B8}$$

provided  $\alpha/\nu$  is not an integer, in which case the derivative (B8) does not exit.

In order to determine the number of stalls  $\lambda$  in any given case, two anemometers are needed with provision for varying the angle  $\alpha$ . If one of the anemometers is on a movable mount such that  $\alpha$  may be varied continuously,  $\lambda$  can be determined unambiguously from equation (B5) or (B8).

When the anemometers are located in fixed positions such that  $\alpha$  is changed by steps, the number of stalls n included in each value of  $\alpha$  must be considered. From equation (B4) and

$$v = \frac{360}{\lambda}$$

there is obtained

$$y = \frac{\alpha \lambda^+}{360} - n \tag{B9}$$

or

$$\lambda^+ = (y + n) \frac{360}{\alpha}$$

for stall zones rotating clockwise. From equation (B7),

$$y = n + 1 - \frac{\alpha \lambda^{-}}{360}$$

or

$$\lambda^{-} = (n + 1 - y) \frac{360}{\alpha}$$
 (B10)

for counterclockwise rotation of the stalled regions.

For various values of  $\alpha$ , y is determined from the oscillograms; then  $\lambda$  may be computed for values of  $n=0,1,2,3,\ldots$  k by use of equations (B9) and (B10) and tabulated as shown in the following table. Unless y is measured quite accurately,  $\lambda$  may not be an integer; however, the nearest integer should be tabulated.

α			$\alpha_1$			
У	У1					
n	0	1	1 2		k	
$\lambda^{+}$	0 1	1 λ <sup>+</sup>	2 1	λ <sup>+</sup>	λ <sup>+</sup>	
λ	$\begin{bmatrix} 0 & \lambda^{-} \\ 1 & 1 & \lambda^{-} \end{bmatrix}$		$2^{\lambda_1}$	3 λ 1	k 1	

$\alpha_2$				$\alpha_{\mathtt{i}}$					
У2			Уi						
0	1	2	3	k	0	1	2	3	k
$0 \lambda^{+}_{2}$	$1^{\lambda^{+}}_{2}$	$2^{\lambda^{+}}_{2}$ $2^{\lambda^{-}}_{2}$	$3^{\lambda^{+}}_{2}$ $3^{\lambda^{-}}_{2}$	k <sup>λ<sup>+</sup></sup> 2 k <sup>λ</sup> 2	ο λ <sup>+</sup> i	λ <sup>+</sup> 1 λ <sup>-</sup> 1 λ	2 λ <sup>+</sup> i 2 λ i	3 <sup>1</sup> i χ <sup>-</sup> i	k i λ <sup>+</sup>

The correct value of the number of stalls  $\lambda$  and their direction of rotation will appear for every value of anemometer spacing  $\alpha$  and the corresponding value of y measured from the oscillogram. If the rotation is clockwise, the correct value of  $\lambda$  will recur in the column  $\lambda^+$ ; if the rotation is counterclockwise, the correct value of  $\lambda$  will recur in the column  $\lambda^-$ . If more than one value of  $\lambda$  recurs, additional values of  $\alpha$  must be tried to determine  $\lambda$ .

Perhaps a more convenient way of determining  $\lambda$  is to plot equations (B9) and (B10). A schematic sketch of such plots of  $\lambda^+$  and  $\lambda^-$  for a particular  $\alpha$  is shown in figure 24. Several values of  $\alpha$  may be included, but only one is shown here for illustrative purposes. By entering the ordinate at the  $\gamma$  value determined from oscillograms, the  $\lambda$  values, read to the nearest integer on the abscissa, occur at the intersections of the  $\gamma$  value and the lines for the integer  $\gamma$ . As described before with the tabular method, the correct value for  $\gamma$  will recur for every value of anemometer spacing  $\gamma$ .

#### Flow Fluctuations

In addition to determining the number of stall zones, the hot-wire anemometer is also used to provide information regarding the magnitude of flow fluctuations during stall. The oscillogram of the hot-wire-anemometer output is a measure of the voltage drop across the wire element of the anemometer probe necessary to maintain it at a fixed resistance and consequently at a constant temperature. The time-averaged value of the anemometer-probe current is proportional to the time-averaged value of voltage drop across the wire element,

$$e = i\Omega$$
 (B11)

The voltage drop e is related to the flow rate  $\rho V$  past the wire element by its heat-transfer characteristics. Reference 15 indicates that the heat-transfer characteristics of the wire element can be correlated satisfactorily by the following formula (King's law):

$$i^{2}\Omega = [C_{1} + f(M)C_{2}\sqrt{\rho V}] (T_{W} - T_{e})$$
 (B12)

The factor f(M) is a function of Mach number, and both  $C_1$  and  $C_2$  are determined by calibration. Solving (B12) for  $\rho V$  results in the following expression:

$$\rho V = \left[ \frac{i^2 \Omega}{C_2 f(M) (T_W - T_e)} - \frac{C_1}{C_2 f(M)} \right]^2$$
 (B13)

By use of the relation  $e = i\Omega$ ,

$$\rho V = \left[ \frac{e^2}{\Omega(T_W - T_e)f(M)C_2} - \frac{C_1}{f(M)C_2} \right]^2$$
 (B14)

If the effect of Mach number of f(M) and possible variation in  $T_e$  during a fluctuation in  $\rho V$  are neglected,

$$\rho V = f(e) \tag{B15}$$

Fluctuations in  $\rho V$  will cause variations in e about some time-averaged value  $\overline{e}$ ; then

$$\rho V = f(e) = f(\overline{e} + \Delta e)$$
 (B16)

Inasmuch as primary interest is in the magnitude of the  $\rho V$  fluctuations compared with the average value, it will be convenient to express the  $\rho V$  fluctuations in terms of the voltage fluctuation across the wire element of the anemometer probe as measured from the oscillograms. Defining

$$\overline{\rho V} \equiv \left[ \frac{\overline{e}^2}{\Omega(T_W - T_e)C_2f(M)} - \frac{C_1}{f(M)C_2} \right]^2 = f(\overline{e})$$
 (B17)

and expanding (Bl6) in a Taylor series give

$$f(e) = f(\overline{e}) + \Delta e \ f'(\overline{e}) + \frac{(\Delta e)^2 f''(\overline{e})}{2!} + \frac{(\Delta e)^3 f'''(\overline{e})}{3!} + \frac{(\Delta e)^4 f''''(\overline{e})}{4!}$$
(B18)

3683

Using

$$f(\overline{e}) = \left(\frac{\overline{e}}{A} - B\right)^2$$
 (B19)

where

$$A = \Omega(T_w - T_e)C_2f(M)$$

$$B = \frac{C_1}{C_2f(M)}$$

(A and B are assumed constant during fluctuation in  $\rho V$ ),

$$f''(e) = \frac{4\overline{e}}{A} \left[ f(\overline{e}) \right]^{\frac{1}{2}}$$

$$f'''(e) = \frac{4[f(\overline{e})]^{\frac{1}{2}}}{A} + \frac{8\overline{e}^{2}}{A^{2}}$$

$$f''''(\overline{e}) = \frac{24\overline{e}}{A^{2}}$$

$$f''''(\overline{e}) = \frac{24}{A^{2}}$$

When (B20) is substituted in (B18),

$$f(e) = f(\overline{e}) + \frac{\overline{e}^4}{A^2} \left[ 4 \left( \frac{\Delta e}{\overline{e}} \right)^2 + 4 \left( \frac{\Delta e}{\overline{e}} \right)^3 + \left( \frac{\Delta e}{\overline{e}} \right)^4 \right] + \frac{\left[ f(\overline{e}) \right] \frac{1}{2}}{A} \left[ 4 \frac{\Delta e}{\overline{e}} + 2 \left( \frac{\Delta e}{\overline{e}} \right)^2 \right]$$
(B21)

results. Rearranging (B21) and dividing both sides by  $f(\overline{e})$  give

$$\frac{f(\overline{e}) - f(e)}{f(\overline{e})} = \frac{\overline{e}^4}{A^2 f(\overline{e})} \left[ 4 \left( \frac{\Delta e}{\overline{e}} \right)^2 + 4 \left( \frac{\Delta e}{\overline{e}} \right)^3 + \left( \frac{\Delta e}{\overline{e}} \right)^4 \right] + \frac{\overline{e}^2}{A[f(\overline{e})]^{\frac{1}{2}}} \left[ 4 \frac{\Delta e}{\overline{e}} + 2 \left( \frac{\Delta e}{\overline{e}} \right)^2 \right] \tag{B22}$$

32

From (B16) and (B17),

$$\frac{f(e) - f(\overline{e})}{f(\overline{e})} = \frac{\rho V - \overline{\rho V}}{\overline{\rho V}} = \frac{\Delta \rho V}{\overline{\rho V}}$$
(B23)

The factor

$$\frac{\overline{e^2}}{A[f(\overline{e})]^{\frac{1}{2}}} = \frac{\overline{e^2}}{A(\overline{e^2} - B)} = \frac{\overline{e^2}}{\overline{e^2} - AB} = \frac{1}{1 - \frac{AB}{\overline{e^2}}}$$
(B24)

From (B19),

$$\frac{AB}{\overline{e}^2} = \frac{C_1 \Omega (T_W - T_e)}{\overline{e}^2}$$

but

$$c_1 = \frac{e_0^2}{\Omega(T_w - T_e)}$$

When  $\rho V = 0$ ,  $e = e_0$ , so

$$\frac{AB}{\overline{e}^2} = \left(\frac{e_0}{\overline{e}}\right)^2$$

and

$$\frac{\overline{e^2}}{A[f(e)]^{\frac{1}{2}}} = \frac{1}{1 - \left(\frac{e_0}{\overline{e}}\right)^2}$$
 (B25)

Substituting (B25) and (B23) in (B22) yields

$$\frac{\triangle \nabla V}{\widehat{PV}} = \left[\frac{1}{1 - \left(\frac{eO}{\overline{e}}\right)^2}\right] \left\{4 \frac{\triangle e}{\overline{e}} + 2\left(\frac{\triangle e}{\overline{e}}\right)^2 + \left[\frac{1}{1 - \left(\frac{eO}{\overline{e}}\right)^2}\right] \left[4\left(\frac{\triangle e}{\overline{e}}\right)^2 + 4\left(\frac{\triangle e}{\overline{e}}\right)^3\right] + \left(\frac{\triangle e}{\overline{e}}\right)^3 + \left(\frac{\triangle e}{\overline{e}}\right)^4\right]\right\}$$
(B26)

A plot of  $\Delta \rho V/\rho V$  against  $\Delta e/\bar{e}$  for various values of  $e_0/\bar{e}$  is presented in figure 25. The mass-flow rate  $\rho V$  is zero when

$$\frac{\Delta e}{\overline{e}} = \frac{e_0 - \overline{e}}{\overline{e}} = \frac{e_0}{\overline{e}} - 1$$

The frequency with which the stall zones passed the hot wire was determined by means of Lissajous figures. Such figures can be formed by putting the hot-wire signal on the y-axis of the oscilloscope and an audio-frequency oscillator on the x-axis. The oscillator is adjusted until the trace on the oscilloscope appears to be a stationary near-circle.

#### REFERENCES

- 1. Grant, Howard P.: Hot Wire Measurements of Stall Propagation and Pulsating Flow in an Axial Flow Inducer-Centrifugal Impeller System. Pratt and Whitney Res. Rep. No. 133, June 1951.
- 2. Iura, T., and Rannie, W. D.: Observations of Propagating Stall in Axial-Flow Compressors. Rep. No. 4, Mech. Eng. Lab., C.I.T., Apr. 1953. (Navy Contract N6-ORI-102, Task Order 4.)
- 3. Emmons, H. W., Pearson, C. E., and Grant, H. P.: Compressor Surge and Stall Propagation. Trans. A.S.M.E., vol. 77, no. 4, May 1955, pp. 455-467; discussion, pp. 467-469.
- 4. Smith, A. G., and Fletcher, P. J.: Observations on the Surging of Various Low-Speed Fans and Compressors. Memo. No. M.219, British N.G.T.E., July 1954.
- 5. Huppert, Merle C., and Benser, William A.: Some Stall and Surge Phenomena in Axial-Flow Compressors. Jour. Aero. Sci., vol. 20, no. 12, Dec. 1953, pp. 835-845.
- 6. Trewby, G. F. A.: British Naval Gas Turbines. Trans. A.S.M.E., vol. 77, no. 4, May 1955, pp. 561-590.
- 7. Sears, W. R.: On Asymmetric Flow in an Axial-Flow Compressor Stage. Jour. Appl. Mech., vol. 20, no. 3, Sept. 1953, pp. 442-443.
- 8. Sears, W. R.: A Theory of "Rotating Stall" in Axial-Flow Compressors. Graduate School Aero. Eng., Cornell Univ., Ithaca (N.Y.). (Contract No. AF 33(038)-21406.)
- 9. Marble, Frank E.: Propagation of Stall in a Compressor Blade Row. Tech. Rep. No. 4, GALCIT, Jan. 1954. (Office Sci. Res., Air Res. and Dev. Command Contract AF 18(600)-178.)
- 10. Stenning, Alan H.: Stall Propagation in Cascades of Airfoils. Jour. Aero. Sci., vol. 21, no. 10, Oct. 1954, pp. 711-713.

NACA TN 3518

11. Ossofsky, Eli: Constant Temperature Operation of the Hot-Wire Anemometer at High Frequency. Rev. Sci. Instr., vol. 19, no. 12, Dec. 1948, pp. 881-889.

- 12. Laurence, James C., and Landes, L. Gene: Auxiliary Equipment and Technique for Adapting the Constant-Temperature Hot-Wire Anemometer to Specific Problems in Air-Flow Measurements. NACA TN 2843, 1952.
- 13. Patterson, John L.: A Miniature Electrical Pressure Gage Utilizing a Stretched Flat Diaphragm. NACA TN 2659, 1952.
- 14. Shepard, Charles E., and Warshawsky, Isidore: Electrical Techniques for Compensation of Thermal Time Lag of Thermocouples and Resistance Thermometer Elements. NACA TN 2703, 1952.
- 15. Lowell, Herman H.: Design and Applications of Hot-Wire Anemometers for Steady-State Measurements at Transonic and Supersonic Airspeeds. NACA TN 2117, 1950.

283

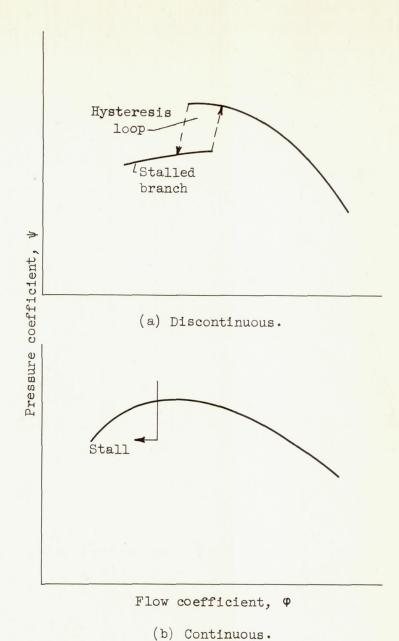


Figure 1. - Compressor performance characteristics.

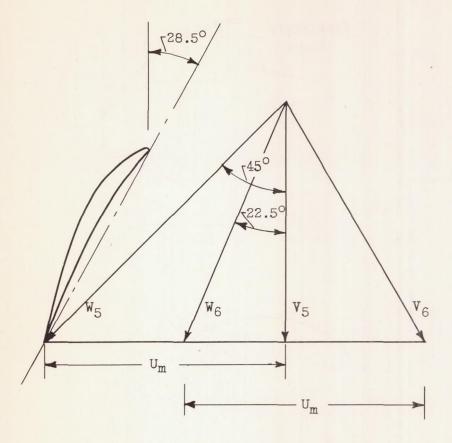


Figure 2. - Vector velocity diagram for 0.9 hub-tip ratio rotor at r = 0.95.

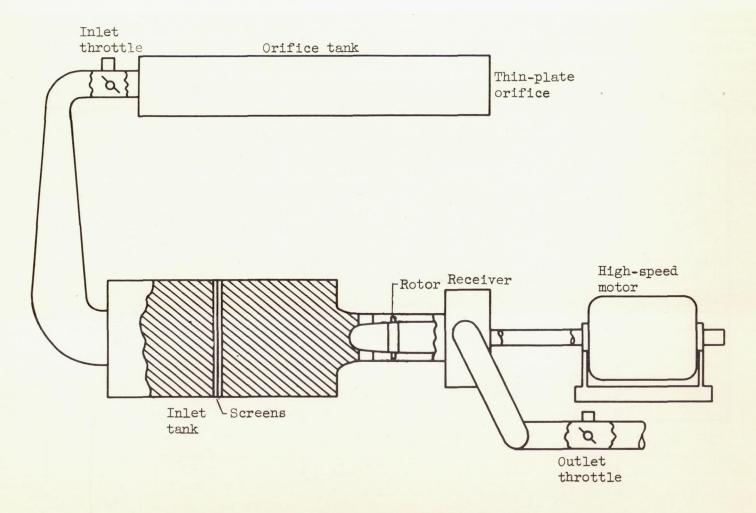


Figure 3. - Schematic diagram of compressor installation.

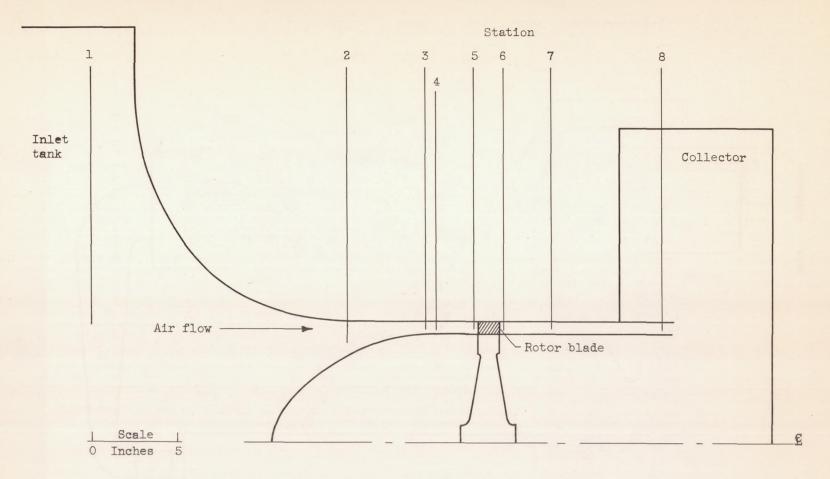


Figure 4. - Axial measuring stations along rotor system.

30 NACA TN 3518

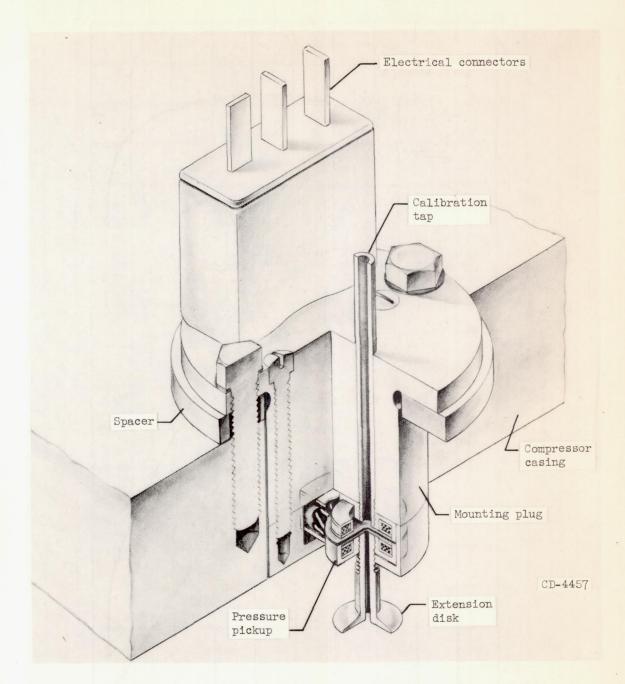


Figure 5. - Installation of pressure pickup in compressor casing.

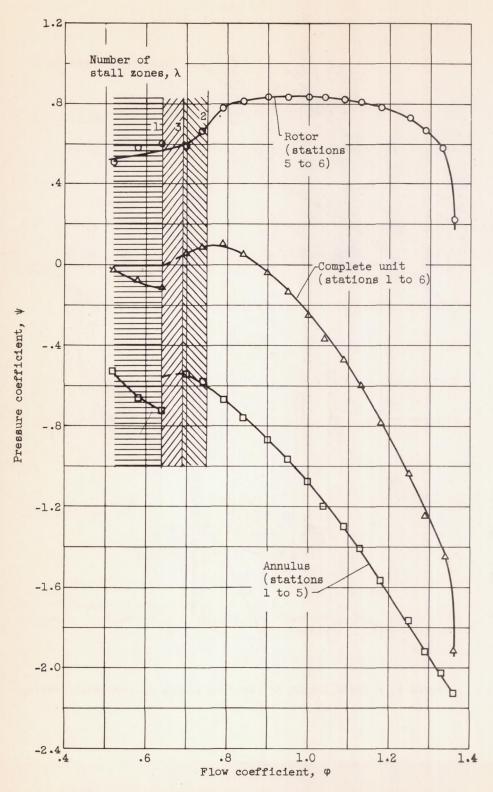


Figure 6. - Static performance characteristics of rotor test system.

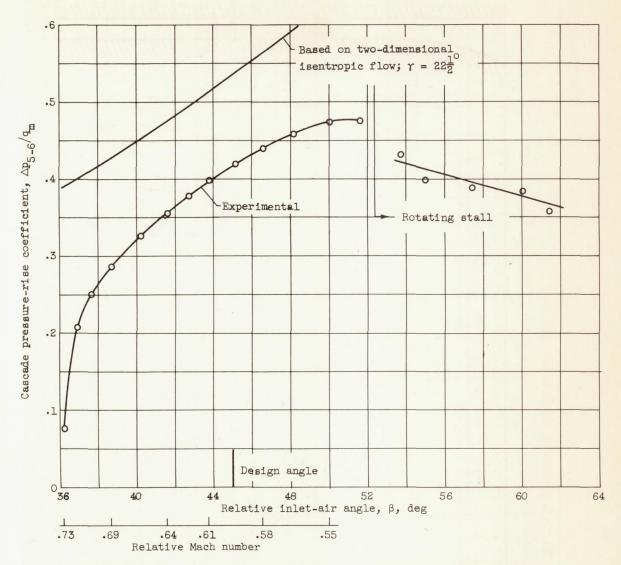


Figure 7. - Rotor pressure-rise characteristic as function of relative inlet-air angle at r = 0.95.

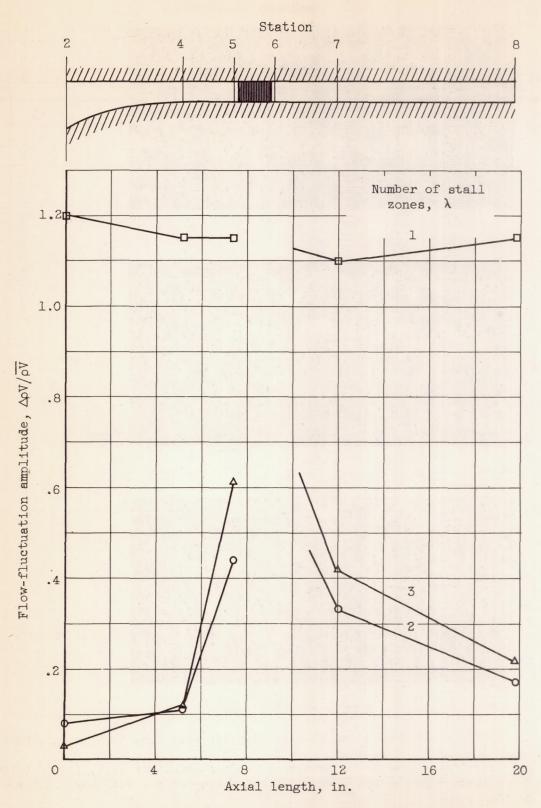
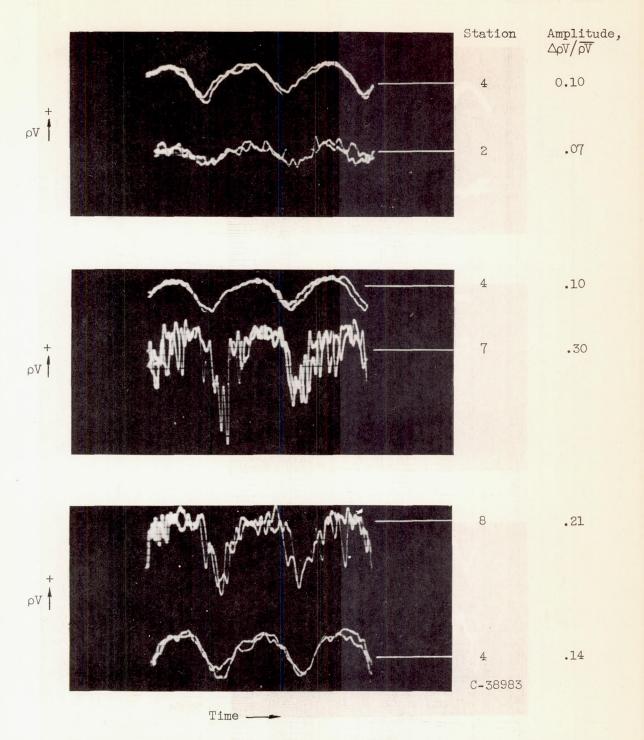


Figure 8. - Flow fluctuations along rotor unit axis.



(a) Two stall zones; stall frequency, 175 cps; flow coefficient, 0.75.

Figure 9. - Hot-wire-anemometer oscillograms at stations 2, 4, 7, and 8 for 0.9 hub-tip ratio rotor. Typical axial survey at r = 0.95 for rotor speed of 8000 rpm.

Amplitude,  $\triangle pV/\overline{pV}$ 

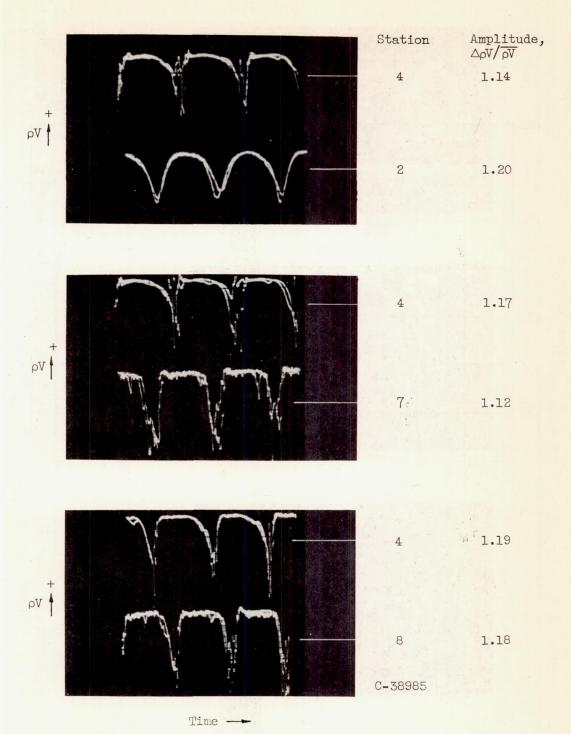
Station

(b) Three stall zones; stall frequency, 276 cps; flow coefficient, 0.68.

Time --

Figure 9. - Continued. Hot-wire-anemometer oscillograms at stations 2, 4, 7, and 8 for 0.9 hub-tip ratio rotor. Typical axial survey at r = 0.95 for rotor speed of 8000 rpm.

3683



(c) One stall zone; stall frequency, 60 cps; flow coefficient, 0.60.

Figure 9. - Concluded. Hot-wire anemometer oscillograms at stations 2, 4, 7, and 8 for 0.9 hub-tip ratio rotor. Typical axial survey at r = 0.95 for rotor speed of 8000 rpm.

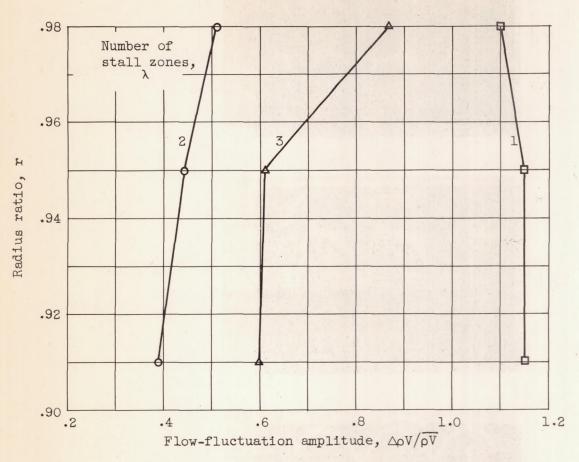
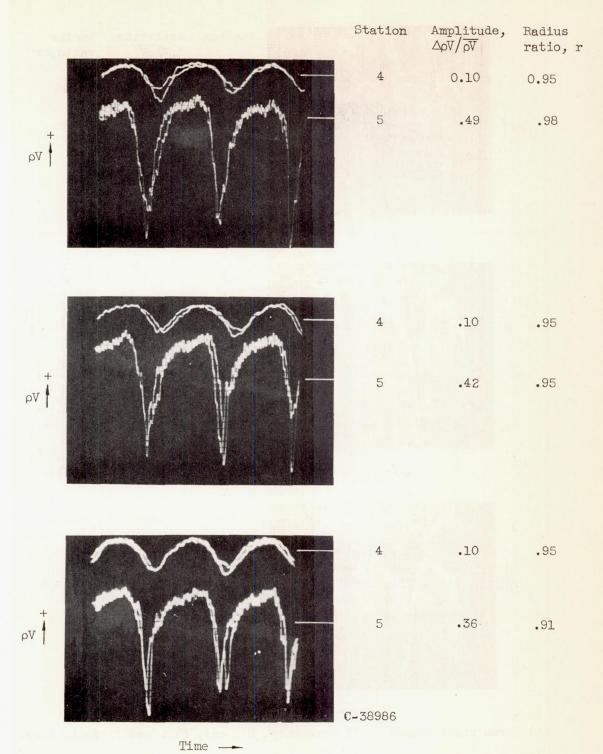
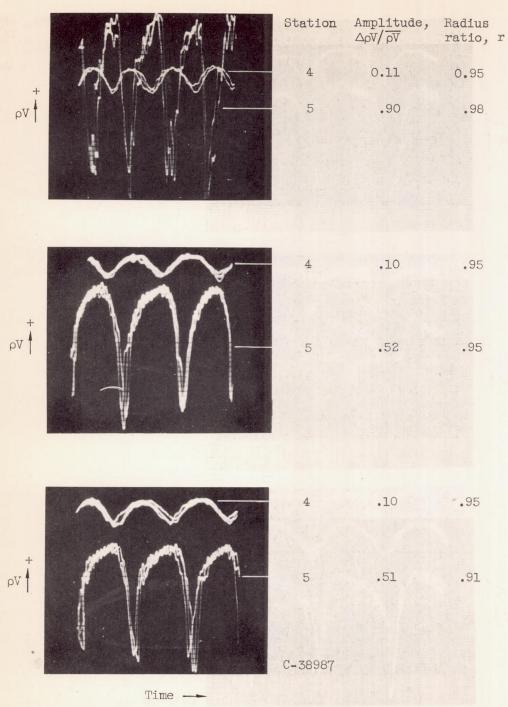


Figure 10. - Flow fluctuations along blade span at station 5.



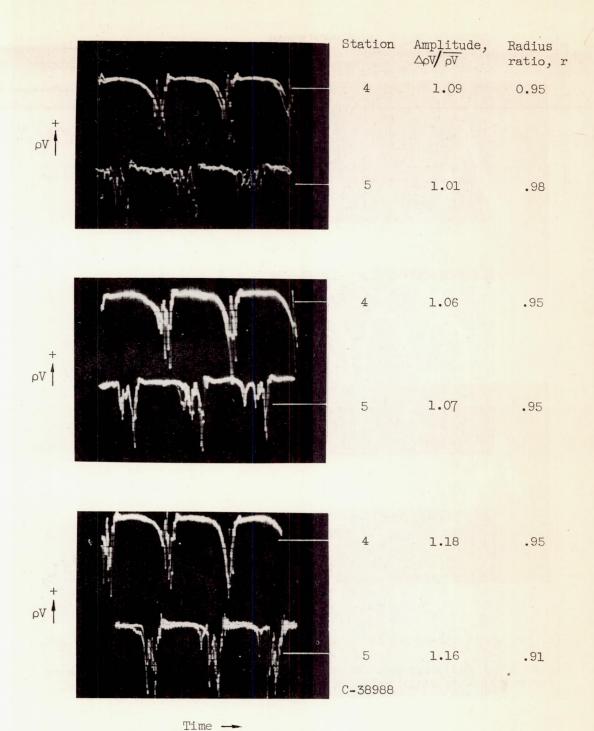
(a) Two stall zones; stall frequency, 175 cps; flow coefficient, 0.75.

Figure 11. - Hot-wire-anemometer oscillograms at stations 4 and 5 for 0.9 hub-tip ratio rotor. Typical radial survey at rotor speed of 8000 rpm.



(b) Three stall zones; stall frequency, 276 cps; flow coefficient, 0.68.

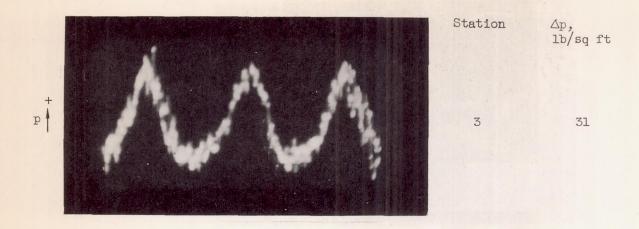
Figure 11. - Continued. Hot-wire-anemometer oscillograms at stations 4 and 5 for 0.9 hub-tip ratio rotor. Typical radial survey at rotor speed of 8000 rpm.

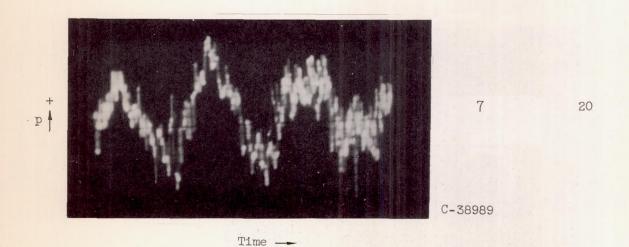


(c) One stall zone; stall frequency, 60 cps; flow coefficient, 0.60.

Figure 11. - Concluded. Hot-wire-anemometer oscillograms at stations 4 and 5 for 0.9 hub-tip ratio rotor. Typical radial survey at rotor speed of 8000 rpm.

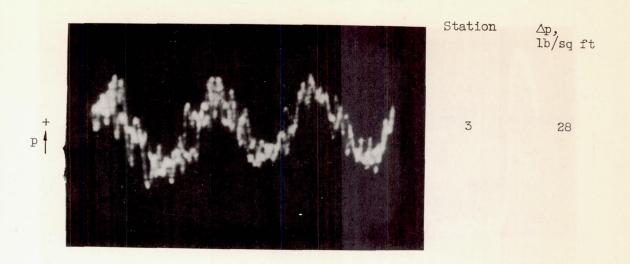
3683

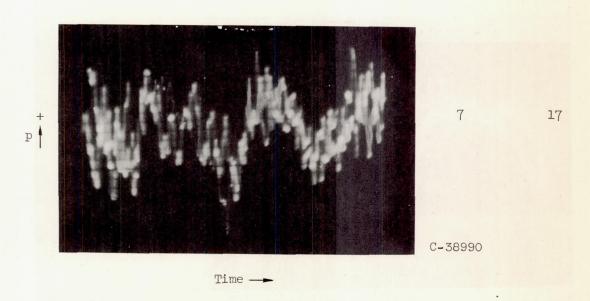




(a) Two stall zones; stall frequency, 175 cps; flow coefficient, 0.705.

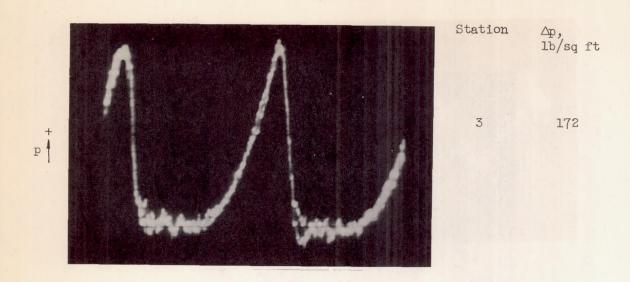
Figure 12. - Oscillograms from high-frequency-response pressure pickups for 0.9 hub-tip ratio rotor at r = 1.0 and rotor speed of 8000 rpm.

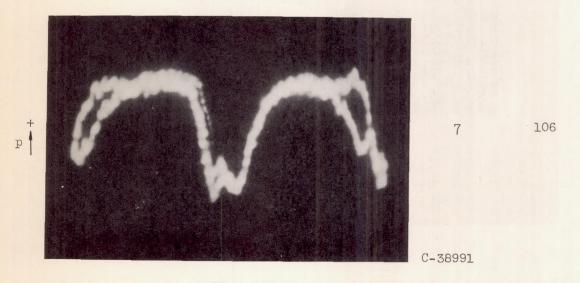




(b) Three stall zones; stall frequency, 276 cps; flow coefficient, 0.68.

Figure 12. - Continued. Oscillograms from high-frequency-response pressure pickups for 0.9 hub-tip ratio rotor at r = 1.0 and rotor speed of 8000 rpm.

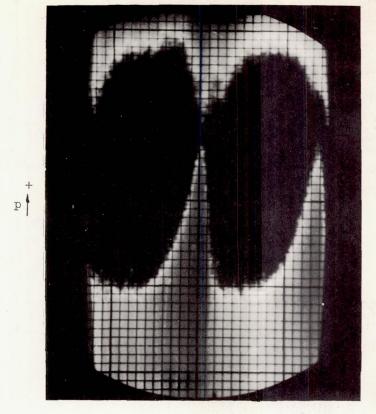




Time \_\_\_

(c) One stall zone; stall frequency, 60 cps; flow coefficient, 0.63.

Figure 12. - Concluded. Oscillograms from high-frequency-response pressure pickups for 0.9 hub-tip ratio rotor at r = 1.0 and rotor speed of 8000 rpm.



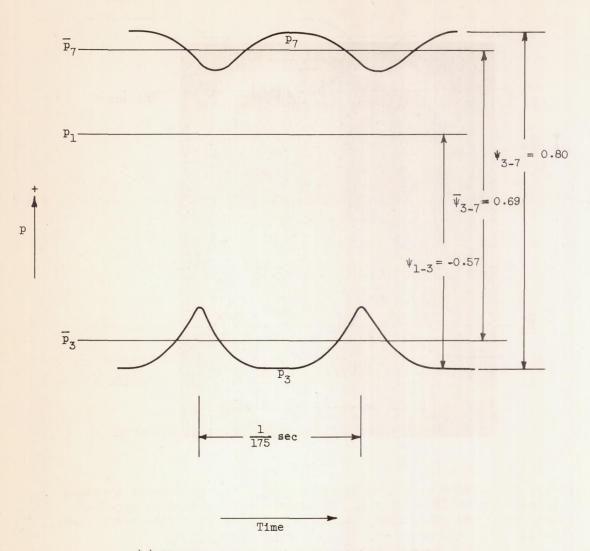
Station 7

Station 3

C-38992

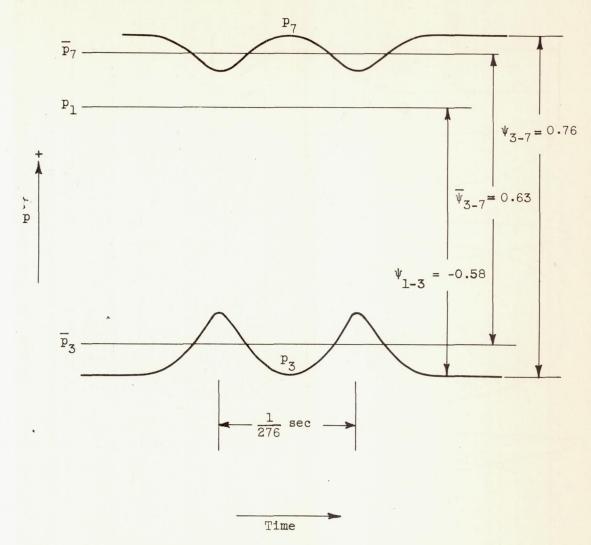
Time \_\_\_

Figure 13. - Phase relation between pressure fluctuations at stations 7 and 3 for 0.9 hub-tip ratio rotor at r = 1.0 and rotor speed of 8000 rpm. One stall zone; stall frequency, 60 cps; flow coefficient, 0.63.



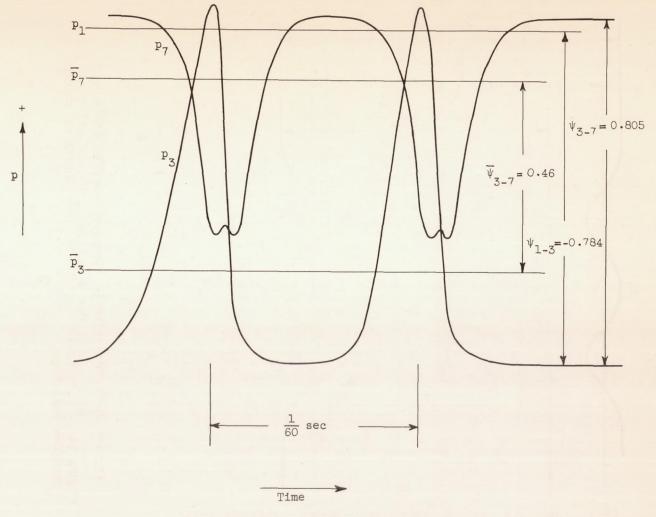
(a) Two stall zones; flow coefficient, 0.705.

Figure 14. - Sketch from oscillogram of static-pressure variation.



(b) Three stall zones; flow coefficient, 0.68.

Figure 14. - Continued. Sketch from oscillogram of staticpressure variation.



(c) One stall zone; flow coefficient, 0.63.

Figure 14. Concluded. Sketch from oscillogram of static-pressure variation.

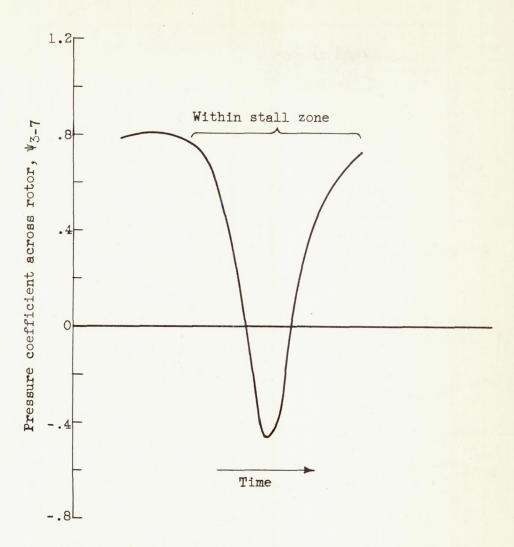


Figure 15. - Variation of pressure coefficient across rotor with time. One stall zone; flow coefficient, 0.63.

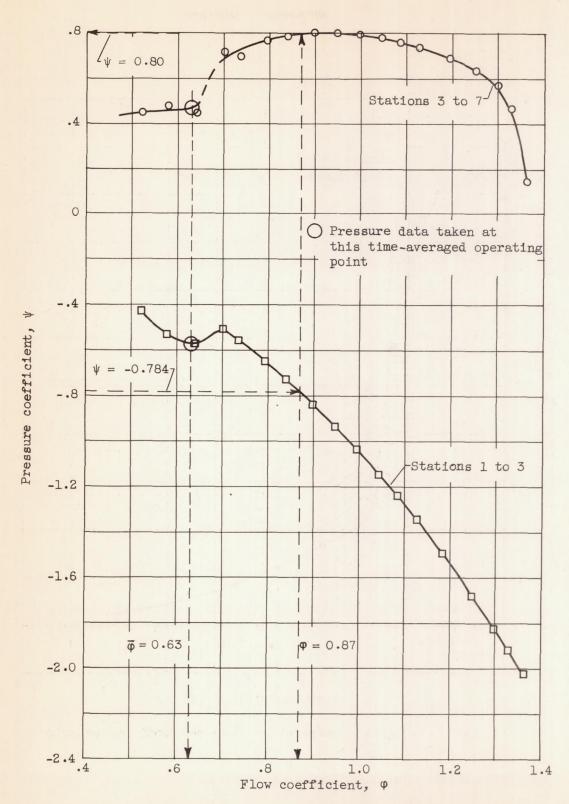


Figure 16. - Static performance characteristics between stations 1 to 3 and 3 to 7.

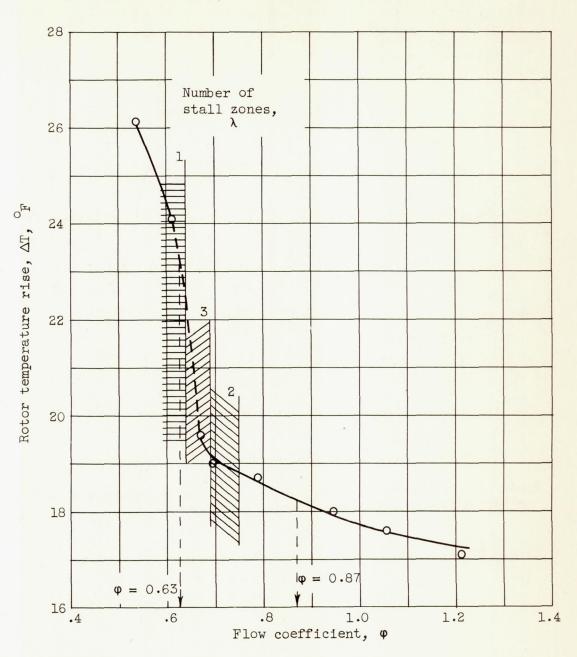


Figure 17. - Average temperature rise measured across rotor.

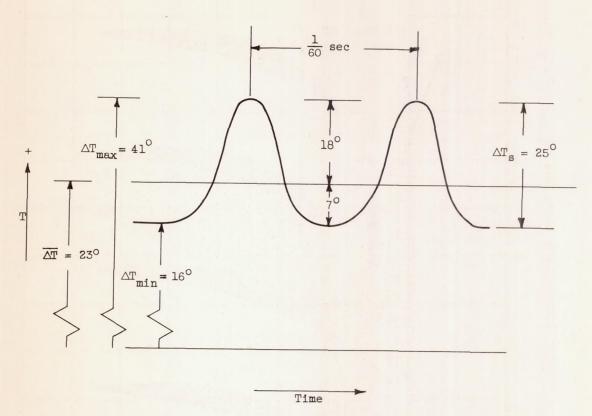


Figure 18. - Variation of temperature rise with time for single-zone stall pattern with flow coefficient of 0.63.

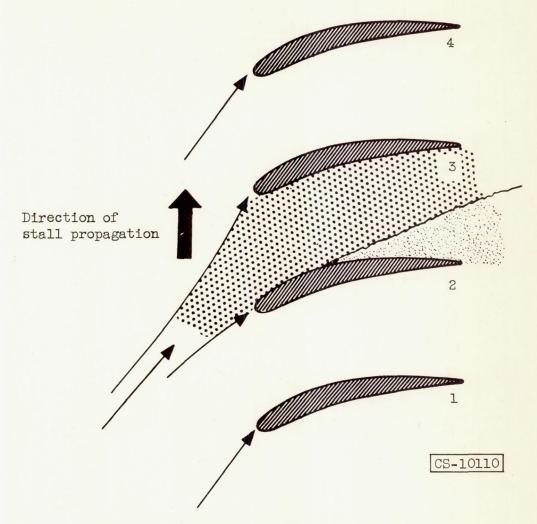


Figure 19. - Stall propagation in cascade.

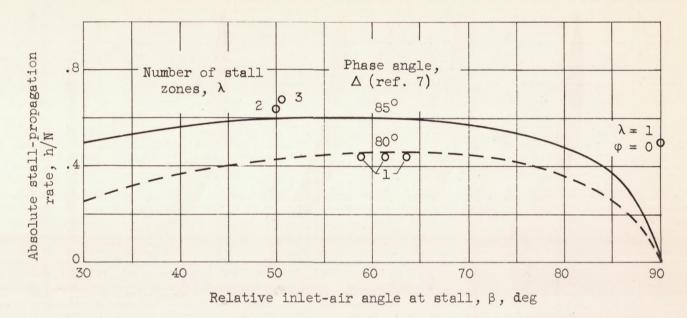


Figure 20. - Comparison of Sears airfoil theory (ref. 7) and experimental absolute stall-propagation rates.

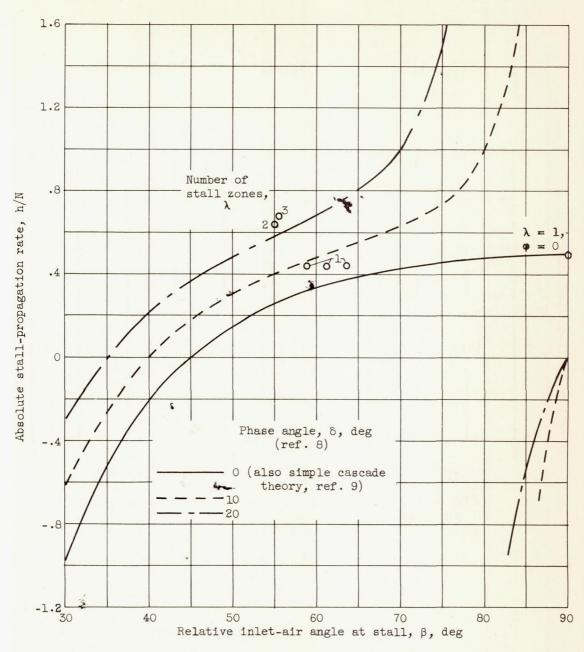


Figure 21. - Comparison of Sears channel theory (ref. 8) and Marble theory (ref. 9) with experimental absolute stall-propagation rates.

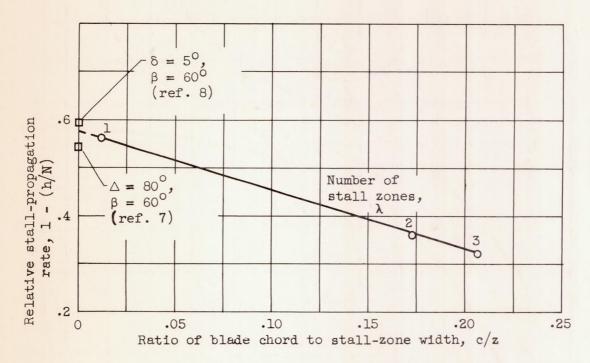
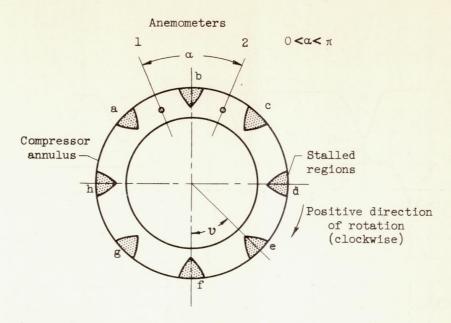
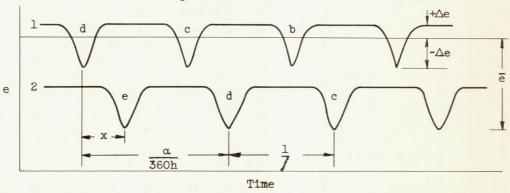


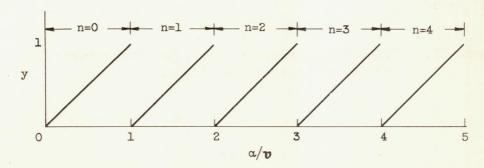
Figure 22. - Effect of stall-zone size on relative stall-propagation rate.



(a) Sketch showing anemometer location and propagating stall in compressor annulus.



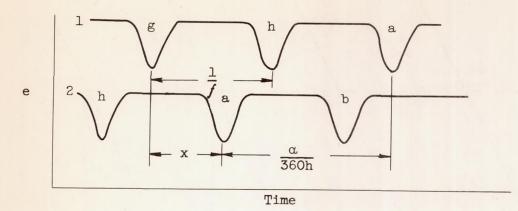
(b) Oscillogram from cathode-ray oscilloscope, clockwise rotation of stall.



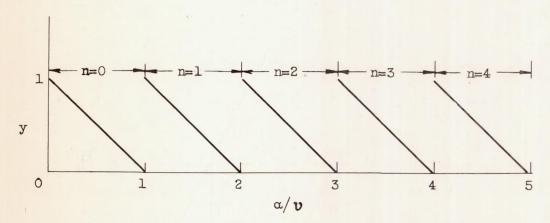
(c) Variation of y with  $\alpha / v$ , clockwise rotation of stall.

Figure 23. - Relations necessary for determining number of propagating stalls.



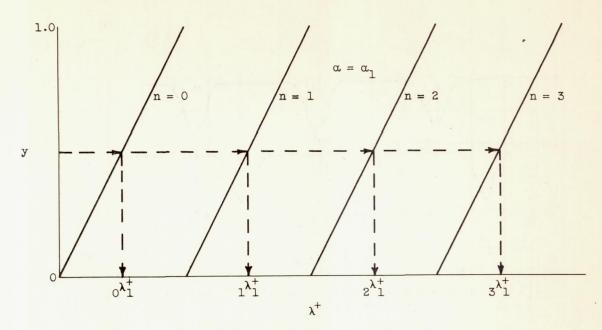


(d) Oscillogram from cathode-ray oscilloscope, counterclockwise rotation of stall.

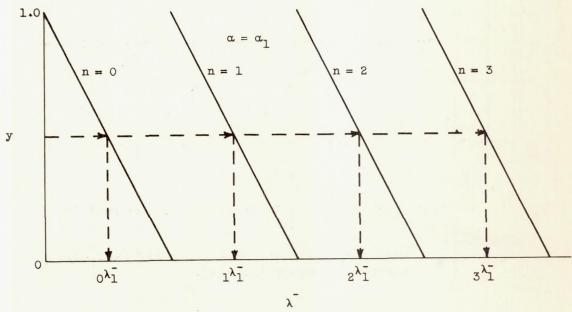


(e) Variation of y with  $\alpha/v$ , counterclockwise rotation of stall.

Figure 23. - Concluded. Relations necessary for determining number of propagating stalls.



(a) Clockwise rotation of stall zone.



(b) Counterclockwise rotation of stall zone.

Figure 24. - Schematic representation of plots useful in determining number of stall zones.

NACA TN 3518 59

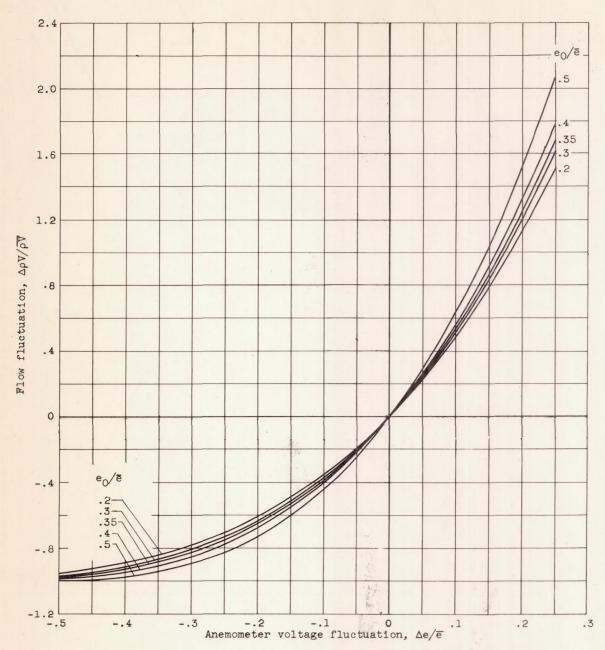


Figure 25. - Variation of weight-flow fluctuations with anemometer voltage fluctuation.